Electrical conductivity of anhydrous and hydrous gabbroic melt under high temperature and high pressure: Implications for the high conductivity anomalies in the region of mid–ocean ridge

Mengqi Wang[1,2], Lidong Dai[1*], Haiying Hu[1*], Ziming Hu[1,2], Chenxin Jing[1,2], Chuanyu Yin[1,2], Song Luo[1,2] and Jinhua Lai[1,2]

[1]*Key Laboratory of High-temperature and High-pressure Study of the Earth's Interior, Institute of Geochemistry, Chinese Academy of Sciences, Guiyang, China*

[2]*University of Chinese Academy of Sciences, Beijing, China*

To be submitted to ***Solid Earth***

February 26th, 2023

*Authors to whom correspondence should be addressed: dailidong@vip.gyig.ac.cn and huhaiying@vip.gyig.ac.cn

11   **Abstract**

12   The electrical conductivity of gabbroic melt with four different water contents

13   (i.e. 0, 2.59 wt%, 5.92 wt% and 8.32 wt%) was measured at temperatures of 873–

14   1373 K and pressures of 1.0–3.0 GPa using YJ–3000t multi–anvil high−pressure

15   apparatus and Solartron−1260 impedance spectroscopy analyzer. At a fixed water

16   content of 2.59 wt%, the electrical conductivity of the sample slightly decreased with

17   increasing pressure at the temperature range of 873–1373 K, and its corresponding

18   activation energy and activation volume were determined as 0.87 ± 0.04 eV and -1.98

19   ± 0.02 cm^3 mole^{-1}, respectively. Under the certain conditions of 873–1373 K and 1.0

20   GPa, the electrical conductivity of the gabbroic melts tends to gradually increase as

21   the rise of water content from 0 to 8.32 wt%, and the activation enthalpy decreases

22   from 0.93 eV to 0.63 eV, accordingly. Furthermore, the functional relation models for

23   the electrical conductivity of gabbroic melts with the variations of temperature,

24   pressure and water content were constructed at high–temperature and high–pressure

25   conditions, respectively. In addition, the dependence relation of the electrical

26   conductivity of melts with the degree of depolymerization was explored under

27   conditions of four different water contents, 1373 K and 1.0 GPa, and three previously

28   available reported results on those of representative calc–alkaline igneous rock melts

29   (i.e. dacitic melt, basaltic melt and andesitic melt) were detailedly compared. In

30   comprehensive combination with our presently acquired electrical conductivity data

31   of gabbroic melt with four different water contents and the available data of

32   polycrystalline olivine, the electrical conductivity of gabbroic melt–olivine system on

33   the variation of volume percentage of anhydrous and hydrous melts was successfully

34   constructed by virtue of the typical Hashin–Shtrikman upper bound model. In light of

35   the electrical conductivity of gabbroic melt–olivine system with the previous MT

36   results, we find that the anhydrous and hydrous gabbroic melts can be employed to

37   reasonably interpret the high conductivity anomalies in the Mohns ridge of the Arctic

38   Ocean.

39   **Keywords: electrical conductivity, gabbroic melt, degree of depolymerization,**

40   **high conductivity anomalies, Mohns ridge**

1 Introduction

The hydrous melt for various rocks and minerals widely exists at active plate tectonic boundaries such as mid–ocean ridge, subduction zone, orogenic belt, etc. (Shen and Forsyth, 1995; White et al., 2001; Wallace, 2005; Wu et al., 2018; Sim et al., 2020; Förster and Selway, 2021; Li et al., 2022; Turner and Langmuir, 2022). For the typical Mohns ridge in the Arctic Ocean, there existed a large amount of high conductivity anomaly phenomena with its correspondent magnitude of 0.08–0.32 S m^{-1} for the gabbro–rich regions have been revealed on the basis of previous magnetotelluric (MT) controlled source electromagnetic (CSEM) results (Johansen et al., 2019).

Previously available researches have indicated that gabbroic and basaltic melts contain a large amount of water, and the water content for the certain type of melt may be discrepant within the different depth ranges of the oceanic crust (Dixon et al., 1995; Almeev et al., 2008; Shaw et al., 2010; Leuthold et al., 2018). Meanwhile, water content is also considered as a crucial ingredient to possibly affect the electrical conductivity of melt, and there are a large number of previously available reported results for the variation of water content on the electrical conductivity of some representative calc–alkaline igneous rock melts at high temperature and high pressure in the recently several years (Ni et al., 2011; Laumonier et al., 2015; Guo et al., 2017; Chen et al., 2018). For example, Ni et al. (2011) measured the electrical conductivity of hydrous basaltic melt within water content range of 0–6.3 wt% at conditions of 1473–1923 K and 2.0 GPa, and they found that the electrical conductivity of basaltic

63 melt with a fixed water content of 6.3 wt% was of the rough 1.0 order of magnitude

64 higher than that of the anhydrous sample. The electrical conductivity of dacitic melt

65 within the water content range of 0–12 wt% was systematically investigated by

66 Laumonier et al. (2015) within temperature range of 673–1623 K and pressures of

67 0.3–3.0 GPa. As pointed out by Laumonier et al. (2015), the high conductivity

68 anomalies in the Uturuncu Volcano could be explained by the presence of hydrous

69 dacitic melt. By virtue of a piston cylinder high–pressure apparatus and sweeping–

70 frequency impedance spectroscopy, Guo et al. (2017) obtained the electrical

71 conductivity data of andesitic melt within the water content range of 0.01–5.90 wt% at

72 conditions of 1164–1573 K and 0.5–1.0 GPa. Their experimental results indicated that

73 the presence of less than 20 vol% of hydrous andesitic melt within the water content

74 range of 6–9 wt% can be used to interpret the high conductivity anomalies beneath the

75 surface of the Uturuncu Volcano. Electrical conductivity measurements of the

76 hydrous leucogranitic melt by Chen et al. (2018) at conditions of 739–1680 K and

77 0.36–2.52 GPa were systematically carried out within the water content range of

78 2.73–11.97 wt%. In comprehensive combination with previous magnetotelluric data

79 in the northwest Himalaya, they considered that water–rich leucogranitic melts with a

80 volume percentage range of 4–16 vol% can be applied to reasonably explain the high

81 conductivity anomalies in these regions.

82   For the natural gabbroic rock, some previously available electrical conductivity

83 results were obtained using the piston–cylinder and multi–anvil high–pressure

84 apparatus at high temperature and high pressure. Sato and Ida (1984) measured the

85 electrical conductivity of the olivine–gabbro containing gabbroic melt at the

86 temperature range from 1123 K to 1473 K and atmospheric pressure, and the effects

87 of ionic diffusion of charge carriers (i.e. sodium, iron, magnesium and/or calcium ions)

88 and geometric structure of melt on the electrical conductivity of olivine–gabbro

89 samples were detailedly explored. The measurements of electrical conductivity for

90 natural gabbro were carried out at conditions of 1023–1423 K and room pressure by

91 Schilling et al. (1997), and they proposed that the electrical conductivity of samples

92 can be enhanced by the increasing volume percentage of gabbroic melt. As for the

93 natural Oman gabbro, the electrical conductivity of gabbroic melt with the volume

94 percentage proportion of 34 % was ~1.0–2.0 orders of magnitude higher than that of

95 melt–free sample within the temperature range from 1073 K to 1523 K and pressures

96 of 0.3–1.0 GPa (Maumus et al., 2005). However, the influence of water content on the

97 electrical conductivity of gabbroic melt at high temperature and high pressure was not

98 investigated in detail. Consequently, it is crucial to make a systematic investigation on

99 the electrical conductivity of gabbroic melt with different water contents at high–

100 temperature and high–pressure conditions.

101   In the present studies, a series of electrical conductivity on the gabbroic melts

102 were systematically performed under conditions of 873–1373 K, 1.0–3.0 GPa and the

103 variation of water content range from 0 to 8.32 wt%. The effects of temperature,

104 pressure and water content on the electrical conductivity of gabbroic melt are deeply

105 explored, and the functional relation models have been successfully established at

106 high–temperature and high–pressure conditions. In conjunction with the degree of

depolymerization, the electrical conductivity of gabbroic melt with different water

contents is compared with that of three representative calc–alkaline igneous rock

melts (i.e. dacitic melt, andesitic melt and basaltic melt). Based on the calculated

electrical conductivity of gabbroic melt–olivine system, its potential geophysical

implication was detailedly discussed in the Mohns ridge of the Arctic Ocean.

2   Experimental procedures

2.1   Sample Preparation

The natural gabbroic rock used in this study was collected from the ophiolite

suite in the region of Ganzi Tibetan autonomous prefecture, Sichuan province, China.

By virtue of the high–temperature quenched melt for the natural rock powder, the

anhydrous and hydrous gabbroic melts are successfully obtained. Firstly, the fresh

natural gabbro was finely crushed and ground into the sample powder with the grain

size of less than 50 μm in an agate mortar. Then, the sample powder was kept in the

furnace at 473 K to remove the absorbed water. To obtain the homogeneously initial

materials for the subsequent electrical conductivity measurement, the powder of

gabbroic rock was melted at the temperature of 1473 K for 1.5 hours and rapidly

quenched in a high–temperature muffle furnace. Further, gabbroic melt was crushed

and ground again into powder with a grain size less than 50 μm and stored in a

vacuum dry furnace at 373 K. To synthesize the hydrous gabbroic melt, the desired

amount of deionized water was added to the powder, and subsequently, the sample

encapsulated in a gold tube using the Lampert–Puk precise welding device. After that,

the starting hydrous gabbroic melts with different water contents were synthesized at

129 conditions of 1373 K and 1.0–3.0 GPa for 12 hours in the YJ−3000t multi−anvil

130 high−pressure apparatus, and all of these obtained samples are homogeneous without

131 any available crystals or bubbles. Detailed hot−pressed sintering assemblage was

132 similar to that previously described by Hu et al. (2022a). Lastly, all of the gabbroic

133 melts were polished into cylinders with diameters of ~4.0–5.0 mm and heights of

134 ~4.0–6.0 mm, and kept in muffle furnace at 423 K for 10 hours to eliminate the

135 absorbed water for subsequent electrical conductivity measurements. The chemical

136 compositions of anhydrous and hydrous gabbroic melts were analyzed by virtue of the

137 electronic probe microscopy analysis (EPMA) at the State Key Laboratory of Ore

138 Deposit Geochemistry, Institute of Geochemistry, Chinese Academy of Sciences,

139 Guiyang, China, as shown in Table 1.

140 **2.2   High−pressure cell and impedance measurements**

141   High−pressure complex impedance measurements for gabbroic melt were

142 performed by using Solartron−1260 impedance spectroscopy analyzer in the YJ−3000t

143 multi−anvil high−pressure apparatus. The cross−section diagram of sample assembly

144 for electrical conductivity measurements was shown in Fig. 1. Before high−pressure

145 cell was assembled, the cubic pressure medium of pyrophyllite with dimension of

146 $32.5 \times 32.5 \times 32.5$ mm^3 and insulation sleeves were baked at 1073 K in a muffle furnace

147 for 5 hours to remove the absorbed water. The sample was placed at the middle of the

148 alumina and magnesia insulation sleeves, and sandwiched with two symmetric nickel

149 electrodes. The electrode was connected with a $Ni_{97}Al_3$ wire to a Solartron−1260

150 impedance spectroscopy analyzer. To shield against external electromagnetism and

151   spurious signal interference, the nickel foil with a thickness of 0.025 mm was installed

152   between the alumina and magnesia sleeves, and linked to the Earth line. Three–layer

153   stainless steel sheets with a total thickness of 0.5 mm were adopted as the heater,

154   which were installed between the cubic pressure medium of pyrophyllite and alumina

155   sleeve. After that, the sample assembly was stored in the vacuum dry furnace at 423 K

156   for at least 12 hours before the electrical conductivity measurements.

157   During the experiment, the pressure was slowly raised with a rate of 1.0 GPa h^{-1}

158   until it reached the desired value, and then the temperature was gradually increased

159   with a speed of 5.0 K min^{-1}. Under predesignated high–temperature and high–

160   pressure condition, impedance spectra of samples were collected in the frequency

161   range of 10^0–10^6 Hz and the applied signal voltage of 1.0 V. To obtain reproducible

162   data, impedance spectra of samples were measured at least two continuously heating–

163   cooling cycles under conditions of 873–1373 K and 1.0–3.0 GPa. The uncertainties of

164   temperature and pressure were less than 5.0 K and 0.1 GPa, respectively. The detailed

165   experimental principles and measurement procedures were described by Dai et al.

166   (2008) and Hu et al. (2022b).

167   **2.3   Determination of the water content**

168   The water content of gabbroic melt before and after the electrical conductivity

169   measurements was performed by virtue of the Vertex−70V and Hyperion−1000

170   vacuum Fourier transform infrared (FT–IR) spectroscopy analyzer. The samples were

171   double–polished up to a thickness of ~50 μm. At least five spectra were conducted on

172   the different regions of transparent sample surfaces and made an average value in

173   order to avoid the heterogeneity effect of water distribution. A detailed experimental

174   method and procedure for the FT–IR measurement was detailedly presented by Hong

175   et al. (2022) and Hu et al. (2022b). For the hydrous gabbroic melts, the signal of the

176   fundamental stretching H_2O vibrational spectroscopy at the peak position of ~3530

177   cm^{-1} of hydroxyl band revealed to be oversaturated, which was similar to the

178   previously obtained results on hydrous dacitic melts reported by Laumonier et al.

179   (2015). The absorbance of gabbroic melt in the water-bearing FTIR spectroscopy at

180   the wavenumber of ~3530 cm^{-1} band is possibly related to the charge carrier species

181   of hydrogen-related defects, such as hydroxyl (OH), free proton et al., which was

182   similar to previously reported hydrous electrical conductivity results on many

183   nominally anhydrous minerals (Huang et al., 2005; Dai and Karato, 2009, 2014a;

184   2020). For water-rich samples, two obviously characteristic peaks were appeared at

185   the correspondent wavenumbers of ~4500 cm^{-1} and ~5200 cm^{-1}, which were

186   representing the hydroxyl band and molecular water band with an available

187   over-saturated state for gabbroic melts, respectively (Stolper, 1982; Dixon et al., 1995;

188   Guo et al., 2017). Thus, we make the integration at the wavenumber ranges of 3000–

189   4000 cm^{-1} and 4000–5800 cm^{-1} for the anhydrous and hydrous samples to precisely

190   determine the water content of gabbroic melts, respectively. The typical FT–IR

191   spectra of gabbroic melt within the wavenumbers range of 2500–5800 cm^{-1} are shown

192   in Fig. 2. The water content of gabbroic melt (C_{melt}) can be worked out by Beer–

193   Lambert law,

194                                  $$C = \omega A/\varepsilon\rho d \qquad (1)$$

$$C_{\text{melt}} = C_{\text{OH}} + C_{\text{H}_2\text{O}} \tag{2}$$

195

196   In here, the signal of ω stands for the molar mass of H_2O (18.02 g mole^{-1}), A stands

197   for the integrated area of absorption spectra (cm^{-2}), ρ stands for the density (g cm^{-3}), d

198   stands for the thickness of thin section (cm), and ε stands for the integral molar

199   absorption coefficient (L mole$^{-1}\cdot$cm^{-2}). As presented the calculated melt density

200   method by Luhr (2001), our density of gabbroic melt is determined as 2.764×10^3 g L^{-1}.

201   Molar absorption coefficients of ε_{OH} and $\varepsilon_{\text{H}_2\text{O}}$ were adopted from Dixon et al.

202   (1995). According to the Equs. 1 and 2, the water contents for three obtained hydrous

203   gabbroic melts were calculated as 2.59 wt%, 5.92 wt% and 8.32 wt% at the

204   wavenumber range from 4000 cm^{-1} to 5800 cm^{-1}, respectively. From Figure 2, it is

205   clear that the absorbance absorption of gabbroic melts in the water-rich FTIR

206   spectroscopy at the wavenumber of ~3530 cm^{-1} band spanning a wide range of water

207   contents look identical. Obviously, the intensity of FT–IR spectra will decrease from

208   water-rich (i.e. its correspondent water content is higher than 2.59 wt%) to water-poor

209   (i.e. anhydrous) gabbroic melts. As displayed in Table 2, there is no significant loss of

210   water for hydrous gabbroic melt during the electrical conductivity experiment. At the

211   same time, the corresponding error bars of each water contents for the initial and

212   recovered gabbroic melts are detailedly included in Table 2.

213   **3   RESULTS**

214   In the present experiments, the electrical conductivity of gabbroic melt with four

215   different water contents (i.e. 0, 2.59 wt%, 5.92 wt% and 8.32 wt%) was measured at

216   temperature range of 873–1373 K and pressures of 1.0–3.0 GPa. The representative

complex impedance spectra of gabbroic melt with the 2.59 wt% water at conditions of

873–1373 K and 2.0 GPa were shown in Fig. 3. According to the theory of *AC*

complex impedance spectra, the impedance spectra of gabbroic melts within the

high-frequency range from $\sim 10^2$–10^3 Hz to 10^6 Hz can be interpreted as the bulk

conduction mechanism (i.e. grain interior), and whereas, the impedance spectra of

sample within the low-frequency range from 10^0 Hz to $\sim 10^2$–10^3 Hz represent the

grain boundary conduction mechanism or the polarization process at sample–electrode

interface (Tyburczy and Roberts (1990), Dai et al. (2008, 2012, 2013, 2014, 2016);

Dai and Karato (2009a, b, c, 2020)). And thus, a series connection of R_S–CPE$_S$ (R_S

and CPE$_S$ represent the resistance and constant–phase element of the gabbroic melt,

respectively) and R_E–CPE$_E$ (R_E and CPE$_E$ represent the interface resistance and

constant–phase element for electrode effect, respectively) were employed as the

equivalent circuit within a relatively lower temperature range of 873–1123 K. As far

as the higher temperature ranges of 1173–1373 K, the equivalent circuit was consisted

of the series connection of one resistance and one parallel resistance with the constant

phase element (CPE). The electrical conductivity of sample can be calculated,

$$\sigma = L/SR \tag{3}$$

In here, *L*, *S* and *R* stand for the length of sample (m), the cross–section area of

electrode (m^2) and the electrical resistance of sample (Ω), respectively. And the

electrical conductivity of gabbroic melt and temperatures conformed to the Arrhenius

relation,

$$\sigma = \sigma_0 \exp(-\Delta H/kT) \tag{4}$$

239   In here, σ_0 stands for the pre–exponential factor (S m^{-1}), k stands for the Boltzmann

240   constant (eV K^{-1}), and T stands for the absolute temperature (K), respectively. All of

241   these fitted parameters for the electrical conductivity of anhydrous and hydrous

242   gabbroic melt under conditions of 873–1373 K and 1.0–3.0 GPa were listed in Table

243   2.

244   For the gabbroic melt with a fixed water content of 2.59 wt%, the electrical

245   conductivity results for two continuously heating–cooling cycles at 873–1373 K and

246   3.0 GPa were shown in Fig. 4. In the first heating cycle within the temperature range

247   of 923–1073 K, the electrical conductivity of sample was slightly deviated with those

248   of subsequent results in the first cooling and second heating–cooling cycles. Whereas,

249   the deviation degree became more and more small and finally overlapped at much

250   higher temperature range of 1123–1373 K. As a whole, the electrical conductivity of

251   sample was almost reproducible in the first cooling and second heating–cooling cycles.

252   And therefore, the electrical conductivity results were acquired by virtue of fitting

253   experimental data during the process of the first cooling and second heating–cooling

254   cycles.

255   **4   Discussions**

256   **4.1   Influence of pressure on electrical conductivity**

257   To identify the effect of pressure on the electrical conductivity of sample, the

258   electrical conductivity of hydrous gabbroic melt was acquired under condition of 873–

259   1373 K, 1.0–3.0 GPa and a fixed water content of 2.59 wt%. As illustrated in Fig. 5,

260   the electrical conductivity of sample and temperature conformed to the Arrhenius

261 relation at a certain water content and pressure condition. In the present studies, a

262 slightly negative dependence relation for the electrical conductivity of hydrous

263 gabbroic melt with a fixed water content of 2.59 wt% on the pressure was observed.

264 The electrical conductivity of sample slightly decreases by around 1.6 times at as

265 pressure enhances from 1.0 GPa to 3.0 GPa at temperature range of 873–1373 K.

266 Accordingly, the pre–exponential factor reduces from 3.02×10^3 S m^{-1} to 6.17×10^2 S

267 m^{-1}, and the activation enthalpy value decreases from 0.85 eV to 0.81 eV,

268 respectively.

269 Furthermore, the influence of pressure on the electrical conductivity of gabbroic

270 melt can be depicted as,

271 $$\sigma = A_0(1-BP) \cdot \exp[-\frac{\Delta U + P\Delta V}{kT}] \tag{5}$$

272 In here, the pre–exponential factor (σ_0) and activation enthalpy (ΔH) of pressure

273 dependence can be illustrated as the relations of $\sigma_0 = A_0(1-BP)$ and $\Delta H = \Delta U + P\Delta V$.

274 All of the listed parameters including ΔU, ΔV, and P stand for the activation energy

275 (eV), the activation volume (cm^3 mole^{-1}) and pressure (GPa), and as well as B is

276 representing a constant, respectively. Furthermore, the electrical conductivity of

277 gabbroic melt along with the variations of temperature, pressure and water content is

278 fitted accordingly and the detailed fitting results are displayed in Table 3. The

279 logarithmic electrical conductivity of gabbroic melt with a fixed water content of 2.59

280 wt% and the inverse temperature follows a good linear relation, which reveals only

281 one main conduction mechanism operating the electrical transport within our

282 experimental temperature and pressure ranges. By virtue of the available pressure–

283   dependent electrical conductivity, we also can extrapolate the relationship between the

284   electrical conductivity of gabbroic melt with a fixed water content of 2.59 wt% and

285   temperature at atmospheric pressure. And then the pre–exponential factor and

286   activation enthalpy at room pressure are calculated as 5177 S m^{-1} and 0.87 eV,

287   respectively. According to Eq. 5 and Table 3, the activation energy and activation

288   volume of gabbroic melt with a fixed water content of 2.59 wt% can be determined as

289   0.87 ± 0.04 eV and -1.98 ± 0.52 cm^3 mole^{-1}.

290   **4.2   Influence of water content on electrical conductivity**

291   For a fixed pressure of 1.0 GPa, the influence of water content on the electrical

292   conductivity of gabbroic melt at temperature range of 873–1373 K is detailedly shown

293   in Fig. 6. The electrical conductivity of gabbroic melt with four different water

294   contents gradually increases with the rise of temperature. For each correspondent

295   water content (i.e. 0, 2.59 wt%, 5.92 wt% and 8.32 wt%), the logarithm of electrical

296   conductivity of the sample and reciprocal temperature follows a good linear relation.

297   On the other hand, when water content of gabbroic melt enhances from 0 to 8.32 wt%,

298   the electrical conductivity of gabbroic melts tends to visibly increase, and whereas the

299   activation enthalpy gradually reduces from 0.93 eV to 0.63 eV, accordingly. In short,

300   our presently acquired electrical conductivity results show a substantial enhancement

301   of water on the electrical conductivity of gabbroic melt, which are also observed

302   among the electrical conductivity of other representative calc–alkaline igneous rock

303   melts in the recent years (Ni et al., 2011; Laumonier et al., 2015; Guo et al., 2017;

304   Chen et al., 2018).

305   The electrical conductivity of hydrous gabbroic melt can be expressed in terms

306   of the charge species concentration dependence of the pre–exponential factor (A),

307   which behaves in an Arrhenius relation,

308    $$\sigma = (A_1 + A_2 \cdot C_w^r) \cdot \exp(\frac{-\Delta H_0 - \alpha C_w^\beta}{RT})$$ (6)

309   In here, C_w is water content of the sample (wt%), ΔH_0 stands for the activation

310   enthalpy, and α, β and r stand for empirical power–law constants. By a non–linear

311   global least–squares method, the electrical conductivity of gabbroic melt with

312   different water contents was fitted and the fitted parameter results were listed in Table

313   4. For the magnitude of water–dependent relation of r (0.43 ± 0.05), it makes clear

314   that the water can dramatically enhance the electrical conductivity of gabbroic melt at

315   conditions of 873–1373 K and 1.0 GPa.

316   **4.3   Comparisons with previous studies**

317   As displayed in Fig. 7, five previously reported results on the electrical

318   conductivity of natural gabbro samples were employed to compare with our

319   absolutely new results for the electrical conductivity of gabbroic melt (Sato and Ida,

320   1984; Schilling et al., 1997; Maumus et al., 2005; Dai et al., 2015; Saito and

321   Bagdassarov, 2018). As a whole, our acquired electrical conductivity results on

322   gabbroic melts are obviously higher than those of natural gabbro at temperature range

323   of 873–1373 K and pressure of 1.0 GPa. Both Sato and Ida (1984) and Schilling et al.

324   (1997) have already performed the electrical conductivity measurements on natural

325   gabbro at high temperature and atmospheric pressure. In case of the occurrence of

326   temperature–induced partial melting, the electrical conductivity of sample will be

327   increased rapidly by several orders of magnitude. However, we find that there is no

328   any relevant information on the water content for their previously reported electrical

329   conductivity results on those of listed melting–bearing natural gabbro samples. The

330   electrical conductivity results of natural gabbro containing 34 vol% melt from

331   Maumus et al. (2005) are much lower than those of our present gabbroic melt, and the

332   obvious discrepancy is possibly caused from the differentiation of the chemical

333   composition and water content of gabbroic melt. In comparison with Saito and

334   Bagdassarov (2018), there is a jump of three orders of magnitude in the electrical

335   conductivity of sample, which is possibly originated from a relatively larger influence

336   of melt volume percentage. As far as the previously reported electrical conductivity of

337   natural gabbro with a relatively lower water content of ~610 ppm and free of any melt

338   by Dai et al. (2015) at pressures of 0.5–2.0 GPa, there is an approximate electrical

339   conductivity result on the anhydrous gabbroic melt to be observed in the present

340   studies. And however, the dependence of electrical conductivity of anhydrous and

341   hydrous gabbroic melts on the temperature, pressure and water content is still scarce

342   under high–temperature and high–pressure conditions until now.

343   It is well known that the gabbroic melt is belonging to one type of representative

344   calc–alkaline igneous rock. As usual, previously available conductivity results

345   confirmed that the electrical conductivity of calc–alkaline igneous rock melts (i.e.

346   dacitic melt, andesitic melt and basaltic melt) is also highly sensitive to the influential

347   factor of the degree of depolymerization at high temperature and high pressure (Ni et

348   al., 2011; Laumonier et al., 2015; Guo et al., 2017). The degree of depolymerization

349   can be characterized by the ratio of non–bridging oxygen ions per tetrahedrally

350   coordinated cation (NBO/T). As pointed out by Mysen et al. (1982), the magnitude of

351   degree of depolymerization on gabbroic melt can be worked out by our above–

352   mentioned EPMA results in Table 1. And the dependence relation of electrical

353   conductivity of gabbroic melts and degree of depolymerization was clearly displayed

354   in Fig. 8 under conditions of four different water contents (i.e. 0, 2.59 wt%, 5.92 wt%

355   and 8.32 wt%), 1373 K and 1.0 GPa. Under constant degree of depolymerization, it

356   makes clears that a relatively lower electrical conductivity is observed in the

357   anhydrous gabbroic melt under condition of 1373 K and 1.0 GPa. With the rise of

358   water content, the electrical conductivity of gabbroic melts dramatically increases,

359   whereas the variation degree for the electrical conductivity gradually reduces. At the

360   same time, we also compared the presently obtained electrical conductivity results for

361   anhydrous and hydrous gabbroic melts with other three representative calc–alkaline

362   igneous melts reported by Ni et al. (2011), Laumonier et al. (2015) and Guo et al.

363   (2017), as detailedly illustrated in Fig. 8. On the base of the previously calculating

364   method for the degree of depolymerization (NBO/T) of melt transforming the detailed

365   EPMA data, the magnitudes in the degree of depolymerization for our present

366   gabbroic melt and other three representative calc–alkaline igneous rock melts (i.e.

367   dacitic melt, andesitic melt and basaltic melt) are 0.65, 0.07, 0.35 and 0.81,

368   respectively. As a whole, the electrical conductivity of four typical calc–alkaline

369   igneous rock melts will increase with the rise of the degree of depolymerization at a

370   fixed water content. As the water content will be enhanced from 0 to 8.32 wt%, the

371   electrical conductivity of each calc–alkaline igneous rock melts will dramatically

372   increase. It is obviously observed that the correspondent variations in the electrical

373   conductivity of calc–alkaline igneous rock melts along the orders from dacitic melt to

374   andesitic melt to gabbroic melt to basaltic melt tend to gradually reduce, and become

375   more and more convergent, accordingly. To my best knowledge, the magnitude in the

376   degree of depolymerization (NBO/T) for the melt sample is highly positive relation

377   with the content variations of alkali–bearing and alkali earth–bearing cations (i.e. Na^+,

378   K^+, Ca^{2+}, Mg^{2+}, etc.) (Mysen et al., 1982; Lee et al., 2003; Di Genova et al., 2015).

379   Just as presented the EPMA results, the total contents of alkali cations and alkali–

380   earth cations are determined as the 11.54 wt% of dacitic melt reported by Laumonier

381   et al. (2015), the 20.41 wt% of andesitic melt reported by Guo et al. (2017), the 30.23

382   wt% of basaltic melt reported by Ni et al. (2011), and as well as the 25.53 wt% of

383   gabbroic melt in this study. And thus, the degree of depolymerization for the calc–

384   alkaline igneous rock melts along the orders from dacitic melt to andesitic melt to

385   gabbroic melt to basaltic melt will gradually increase, accordingly. On the other hand,

386   previous electrical conductivity results have confirmed that the main charge carriers

387   of the calc–alkaline igneous melts are alkali cations and alkali–earth cations at high

388   temperature and high pressure (Ni et al., 2011; Laumonier et al., 2015; Guo et al.,

389   2017; Chen et al., 2018). And thus, the influence of the degree of depolymerization on

390   the electrical conductivity of melt is possibly caused from the concentration of the

391   alkali cations and alkali–earth cations. Accordingly, the electrical conductivity of

392   calc–alkaline igneous melts will gradually increase with the rise of alkali cations and

393   alkali–earth cations along the orders from dacitic melt to andesitic melt to gabbroic

394   melt to basaltic melt. In sum, as followed the orders from dacitic melt to andesitic

395   melt to gabbroic melt to basaltic melt, it is very reasonable that the electrical

396   conductivity of calc–alkaline igneous melts will be gradually enhanced with the rise

397   of degree of depolymerization (NBO/T) under conditions of 1373 K and 1.0 GPa.

5   Geophysical implications

399   As a typical active plate geotectonic boundary, previously available

400   magnetotelluric results have already revealed that the phenomenon of high

401   conductivity anomalies is widespread distributed in the region of mid–ocean ridge

402   (Key et al., 2013; Miensopust et al., 2014). For the representative Mohns ridge of the

403   Arctic Ocean, there widely exist a large number of high conductive layers with their

404   conductivity magnitude within the range of ~0.08–0.32 S m^{-1} at the correspondent

405   depths from 4 km to 7 km (Johansen et al., 2019). All of these acquired seismic and

406   gravitational survey datasets have confirmed that various volume percentages of

407   gabbroic melt widely outcropped in the Mohns ridge of the Arctic Ocean at the depths

408   of ~4–11 km (Géli et al., 1994; Conley and Dunn, 2011). And therefore, the high

409   conductivity anomalies in the Mohns ridge of the Arctic Ocean are possibly correlated

410   with the gabbroic melt at high temperature and high pressure. In conjunction with our

411   presently obtained experimental results on the electrical conductivity of anhydrous

412   and hydrous gabbroic melts at conditions of 873–1373 K and 1.0–3.0 GPa, the typical

413   Hashin–Shtrikman upper bound model and previously available magnetotelluric

414   results, the electrical conductivity of gabbroic melt–olivine system was constructed in

415   detail, as displayed in Fig. 9. All of these influential ingredients including water

416   content and volume percentage were comprehensively considered. During the process

417   of the expansion of mid–ocean ridge caused by the rapid upwelling of asthenosphere

418   mantle, the geothermal distribution exhibited an abnormal behavior in the Mohns

419   ridge of the Arctic Ocean. As pointed out by Johansen et al. (2019), the temperature

420   on the top gabbro layer is approximate to 1373 K along the ultraslow–spreading

421   Arctic mid–ocean Mohns ridge region. In addition, the effect of pressure on the

422   electrical conductivity of gabbroic melt is rather feeble, and it can be neglected.

423   For the representative Mohns ridge of the Arctic Ocean, previously available

424   petrological and geochemical results have already revealed that the range of water

425   content for the crustal rock and melt in the Mohns ridge is ~0.25–2.64 wt% (Neumann

426   and Schilling, 1984; Poreda et al., 1986). The electrical conductivity results of

427   gabbroic melt with two different water contents (anhydrous and a water content of

428   2.59 wt%) are selected from our present studies. The electrical conductivity of olivine

429   at 1373 K and 1.0 GPa is properly extrapolated from the available experimental data

430   of polycrystalline olivine under conditions of 160 ppm wt water content, 873–1273 K

431   and 4.0–10.0 GPa reported by Dai and Karato (2014b). On the variation of volume

432   percentage for the gabbroic melt, the electrical conductivity of a gabbroic melt–

433   olivine system (σ_{HS+}) can be expressed as (Hashin and Shtrikman, 1962),

434 $$\sigma_{HS+} = \sigma_{melt} + [(1-X_{melt})\cdot[(\sigma_{olivine}-\sigma_{melt})^{-1} + X_{melt}/(3\cdot\sigma_{melt})]]^{-1} \qquad (7)$$

435 In here, the signals of σ_{melt} and $\sigma_{olivine}$ stand for the electrical conductivity of gabbroic

436 melt from the present study and that of polycrystalline olivine with a certain water

437   content of 160 ppm wt from Dai and Karato (2014b), respectively; X_{melt} stands for the

438   volume percentage of gabbroic melt.

439   The electrical conductivity of gabbroic melt–olivine system with different

440   volume percentage of gabbroic melt was successfully worked out at 1373 K and 1.0

441   GPa, as displayed in Fig. 9. For the gabbroic melt–olivine system with a certain

442   volume percentage of gabbroic melt, the electrical conductivity increases with the rise

443   of water content in gabbroic melt. As far as the gabbroic melt containing a fixed water

444   content, the electrical conductivity of gabbroic melt–olivine system gradually

445   enhances as the volume percentage of gabbroic melt increases. As pointed out by

446   Johansen et al. (2019), the range of electrical conductivity for the HCL in the Mohns

447   ridge is ~0.08–0.32 S m^{-1}, as displayed in the orange region of Fig. 9. For the

448   anhydrous gabbroic melt, the required volume percentage for the high conductivity

449   anomalies the ultraslow-spreading Arctic mid-ocean Mohns ridge region falls within

450   the range of ~2.93–34.69 vol%, which is in good agreement with previously inferred

451   results from geophysical observations (Géli et al., 1994; Conley and Dunn, 2011).

452   When the water content of gabbroic melt increases, the required volume percentage

453   for the HCL reduces accordingly. As for the gabbroic melt with a relatively high water

454   content of 2.59 wt%, its volume percentage range of ~2.63–23.63 vol% is enough to

455   explain the high conductivity anomalies. In summary, the high conductivity anomalies

456   in the Mohns ridge of the Arctic Ocean could be interpreted by the anhydrous and

457   hydrous gabbroic melt, and our present electrical conductivity results for gabbroic

458   melt with different water contents can provide an important constraint for the water

459 content and volume percentage of gabbroic melt at depth range of ~4–7 km within the

460 Mohns ridge region of the Arctic Ocean.

Conclusions

461

462 In the present studies, the electrical conductivity of gabbroic melt with different

463 water contents of 0–8.32 wt% were measured at temperatures of 873–1373 K and

464 pressures of 1.0–3.0 GPa. For the gabbroic melt with a fixed water content of 2.59

465 wt%, the electrical conductivity of the sample decreases slightly with the rise of

466 pressure, and its corresponding activation energy and activation volume are

467 determined as 0.87 ± 0.04 eV and -1.98 ± 0.02 cm^3 mole^{-1}, respectively. When water

468 content of gabbroic melt enhances from 0 to 8.32 wt% under the certain conditions of

469 873–1373 K and 1.0 GPa, the electrical conductivity of gabbroic melts tends to visibly

470 increase, and whereas the activation enthalpy gradually reduces from 0.93 eV to 0.63

471 eV, accordingly. Furthermore, the functional relation models for the electrical

472 conductivity of gabbroic melt with the variations of temperature, pressure and water

473 content are constructed at high–temperature and high–pressure conditions,

474 respectively. By virtue of typical Hashin–Shtrikman upper bound model, the electrical

475 conductivity of gabbroic melt–olivine system on the variation of melt volume

476 percentage is calculated under the conditions of four different water contents of

477 gabbroic melt (i.e. 0, 2.59 wt%, 5.92 wt% and 8.32 wt%), 1373 K and 1.0 GPa, which

478 can be employed to reasonably explain the high conductivity anomalies in the Mohns

479 ridge of the Arctic Ocean observed by the previously available field MT results.

480   *Data availability.* The data that support the findings of this study are available

481   from the first author upon reasonable request.

482   *Acknowledgements.* This research was financially supported by the NSF of China

483   (grant number 42072055 and 42274137) and the Youth Innovation Promotion

484   Association of CAS (grant number 2019390).

485   *Declaration of competing interest.* The authors declare that they have no

486   conflict of interest.

References

Almeev, R., Holtz, F., Koepke, J., Haase, K., and Devey, C.: Depths of partial crystallization of H_2O-bearing MORB: Phase equilibria simulations of basalts at the MAR near Ascension Island (7–11°S), J. Petrol., 49, 25–45, 2008.

Chen, J. Y., Gaillard, F., Villaros, A., Yang, X. S., Laumonier, M., Jolivet, L., Unsworth, M., Hashim, L., Scaillet, B., and Richard, G.: Melting conditions in the modern Tibetan crust since the Miocene, Nat. Commun., 9, 3515, https://doi.org/10.1038/s41467-018-05934-7, 2018.

Conley, M. M. and Dunn, R. A.: Seismic shear wave structure of the uppermost mantle beneath the Mohns Ridge, Geochem. Geophys. Geosyst., 12, Q0AK01, https://doi.org/10.1029/2011GC003792, 2011.

Dai, L. D., Li, H. P., Hu, H. Y., and Shan, S. M.: Experimental study of grain boundary electrical conductivities of dry synthetic peridotite under high-temperature, high-pressure, and different oxygen fugacity conditions, J. Geophys. Res. Solid Earth, 113, B12211, https://doi.org/10.1029/2008JB005820, 2008.

Dai, L. D. and Karato, S. I.: Electrical conductivity of pyrope-rich garnet at high temperature and high pressure, Phys. Earth Planet. Inter., 176, 83–88, 2009a.

Dai, L. D. and Karato, S. I.: Electrical conductivity of orthopyroxene: Implications for the water content of the asthenosphere, Proc. Jpn. Acad. Ser. B, 85, 466–475, 2009b.

Dai, L. D. and Karato, S. I.: Electrical conductivity of wadsleyite at high temperatures

509   and high pressures, Earth Planet. Sci. Lett., 287, 277–283, 2009c.

510   Dai, L. D., Li, H. P., Hu, H. Y., Shan, S. M., Jiang, J. J., and Hui, K. S.: The effect of

511   chemical composition and oxygen fugacity on the electrical conductivity of dry

512   and hydrous garnet at high temperatures and pressures, Contrib. Mineral. Petrol.,

513   163, 689–700, 2012.

514   Dai, L. D., Li, H. P., Hu, H. Y., Jiang, J. J., Hui, K. S., and Shan, S. M.: Electrical

515   conductivity of $Alm_{82}Py_{15}Grs_3$ almandine-rich garnet determined by impedance

516   spectroscopy at high temperatures and high pressures, Tectonophysics, 608,

517   1086–1093, 2013.

518   Dai, L. D., Hu, H. Y., Li, H. P., Jiang, J. J., and Hui, K. S.: Effects of temperature,

519   pressure and chemical composition on the electrical conductivity of granite and

520   its geophysical implications, Am. Mineral., 99, 1420–1428, 2014.

521   Dai, L. D. and Karato, S. I.: Influence of oxygen fugacity on the electrical

522   conductivity of olivine under hydrous conditions: Implications for the

523   mechanism of conduction. Phys. Earth Planet. Inter., 232, 57–60, 2014a.

524   Dai, L. D. and Karato, S. I.: The effect of pressure on the electrical conductivity of

525   olivine under the hydrogen-rich conditions, Phys. Earth Planet. Inter., 232, 51–56,

526   2014b.

527   Dai, L. D., Hu, H. Y., Li, H. P., Hui, K. S., Jiang, J. J., Li, J., and Sun, W. Q.:

528   Electrical conductivity of gabbro: The effects of temperature, pressure and

529   oxygen fugacity, Eur. J. Mineral., 27, 215–224, 2015.

530   Dai, L. D., Hu, H. Y., Li, H. P., Wu, L., Hui, K. S., Jiang J. J., and Sun, W. Q.:

Influence of temperature, pressure, and oxygen fugacity on the electrical

conductivity of dry eclogite, and geophysical implications, Geochem. Geophys.

Geosyst., 17, 2394–2407, 2016.

Dai, L. D. and Karato, S. I.: Electrical conductivity of Ti–bearing hydrous olivine

aggregates at high temperature and high pressure, J. Geophys. Res. Solid Earth,

125, e2020JB020309, https://doi.org/10.1029/2020JB020309, 2020.

Di Genova, D., Morgavi, D., Hess, K. U., Neuville, D. R., Borovkov, N., Perugini, D.,

and Dingwell, D. B.: Approximate chemical analysis of volcanic glasses using

Raman spectroscopy, J. Raman Spectrosc., 46, 1235–1244, 2015.

Dixon, J. B., Stolper, E. M., and Holloway, J. R.: An experimental study of water and

carbon dioxide solubilities in mid-ocean ridge basaltic liquids. Part I: Calibration

and solubility models, J. Petrol., 36, 1607–1631, 1995.

Förster, M. W. and Selway, K.: Melting of subducted sediments reconciles

geophysical images of subduction zones, Nat. Commun., 12, 1320,

https://doi.org/10.1038/s41467-021-21657-8, 2021.

Géli, L., Renard, V., and Rommevaux, C.: Ocean crust formation processes at very

slow spreading centers: A model for the Mohns Ridge, near 72°N, based on

magnetic, gravity, and seismic data, J. Geophys. Res. Solid Earth, 99, 2995–3013,

1994.

Guo, X., Li, B., Ni, H. W., and Mao, Z.: Electrical conductivity of hydrous andesitic

melts pertinent to subduction zones, J. Geophys. Res. Solid Earth, 122, 1777–

1788, 2017.

553   Hashin, Z. and Shtrikman, S.: A variation approach to the theory of effective magnetic

554   permeability of multiphase materials, J. Appl. Phys., 33, 3125–3131, 1962.

555   Hong, M. L., Dai, L. D., Hu, H. Y., Yang, L. F. and Zhang, X. Y.: Pressure-induced

556   structural phase transitions in natural kaolinite investigated by Raman

557   spectroscopy and electrical conductivity, Am. Mineral., 107, 385–394, 2022.

558   Hu, H. Y., Dai, L. D., Sun, W. Q., Wang, M. Q., and Jing, C. X.: Constraints on fluids

559   in the continental crust from laboratory-based electrical conductivity

560   measurements of plagioclase, Gondwana Res., 107, 1–12, 2022a.

561   Hu, H. Y., Jing, C. X., Dai, L. D., Yin, C. Y. and Chen, D. M.: Electrical conductivity

562   of siderite and its implication for high conductivity anomaly in the slab-mantle

563   wedge interface, Front. Earth Sci., 10, 985740,

564   https://doi.org/10.3389/feart.2022.985740, 2022b.

565   Huang, X. G., Xu, Y. S., and Karato S. I.: Water content in the transition zone from

566   electrical conductivity of wadsleyite and ringwoodite, Nature, 434, 746–749,

567   2005.

568   Johansen, S. E., Panzner, M., Mittet, R., Amundsen, H. E. F., Lim, I., Vik, E., Landrø,

569   M., and Arntsen, B.: Deep electrical imaging of the ultraslow-spreading Mohns

570   ridge, Nature, 567, 379–383, 2019.

571   Key, K., Constable, S., Liu, L. J., and Pommier, A.: Electrical image of passive mantle

572   upwelling beneath the northern East Pacific Rise, Nature, 495, 499–502, 2013.

573   Laumonier, M., Gaillard, F., and Sifre, D.: The effect of pressure and water

574   concentration on the electrical conductivity of dacitic melts: Implication for

575   magnetotelluric imaging in subduction areas, Chem. Geol., 418, 66–76, 2015.

576   Lee, S. K., Mysen, B. O., and Cody, G. D.: Chemical order in mixed-cation silicate

577   glasses and melts, Phys. Rev. B, 68, 214206,

578   https://doi.org/10.1103/PhysRevB.68.214206, 2003.

579   Leuthold, J., Lissenberg, C. J., O'Driscoll, B., Karakas, O., Falloon, T., Klimentyeva,

580   D. N., and Ulmer, P.: Partial melting of lower oceanic crust gabbro: Constraints

581   from poikilitic clinopyroxene primocrysts, Front. Earth Sci., 6, 15,

582   https://doi.org/10.3389/feart.2018.00015, 2018.

583   Li, G. H., Gao, Y., Zhou, Y. Z., Ju, C. H., Shi, Y. T., and Cui, Q. H.: A low-velocity

584   layer atop the mantle transition zone beneath the western Central Asian Orogenic

585   Belt: Upper mantle melting induced by ancient slab subduction, Earth Planet. Sci.

586   Lett., 578, 117287, https://doi.org/10.1016/j.epsl.2021.117287, 2022.

587   Luhr, J. F.: Glass inclusions and melt volatile contents at Parícutin Volcano, Mexico,

588   Contrib. Mineral. Petrol., 142, 261–283, 2001.

589   Maumus, J., Bagdassarov, N., and Schmeling, H.: Electrical conductivity and partial

590   melting of mafic rocks under pressure, Geochim. Cosmochim. Ac., 69, 4703–

591   4718, 2005.

592   Miensopust, M. P., Jones, A. G., Hersir, G. P., and Vilhjálmsson, A. M.: The

593   Eyjafjallajökull volcanic system, Iceland: Insights from electromagnetic

594   measurements, Geophys. J. Int., 199, 1187–1204, 2014.

595   Mysen, B. O., Virgo, D., and Seifert, F. A.: The structure of silicate melts:

596   Implications for chemical and physical properties of natural magma, Rev.

597   Geophys., 20, 353–383, 1982.

598 Neumann, E. R. and Schilling, J. G.: Petrology of basalts from the Mohns–Knipovich

599   Ridge; the Norwegian–Greenland Sea, Contrib. Mineral. Petrol., 85, 209–223,

600   1984.

601 Ni, H. W., Keppler, H., and Behrens, H.: Electrical conductivity of hydrous basaltic

602   melts: Implications for partial melting in the upper mantle, Contrib. Mineral.

603   Petrol., 162, 637–650, 2011.

604 Poreda, R., Schilling, J. G., and Craig, H.: Helium and hydrogen isotopes in ocean–

605   ridge basalts north and south of Iceland, Earth Planet. Sci. Lett., 78, 1–17, 1986.

606 Saito, S. and Bagdassarov, N. S: Laboratory measurements of electrical conductivity

607   in a gabbro of the Oman ophiolite at high–pressures and high–temperatures:

608   Implications for interpretation of resistivity structures of lower oceanic crust, J.

609   Mineral. Petrol. Sci., 113, 112–117, 2018.

610 Sato, H. and Ida, Y.: Low frequency electrical impedance of partially molten gabbro:

611   the effect of melt geometry on electrical properties, Tectonophysics, 107, 105–

612   134, 1984.

613 Schilling, F. R., Partzsch, G. M., Brasse, H., and Schwarz, G.: Partial melting below

614   the magmatic arc in the central Andes deduced from geoelectromagnetic field

615   experiments and laboratory data, Phys. Earth Planet. Inter., 103, 17–31, 1997.

616 Shaw, A. M., Behn, M. D., Humphris, S. E., Sohn, R. A., and Gregg, P. M.: Deep

617   pooling of low degree melts and volatile fluxes at the 85°E segment of the

618   Gakkel Ridge: Evidence from olivine-hosted melt inclusions and glasses, Earth

Planet. Sci. Lett., 289, 311–322, 2010.

Shen, Y. and Forsyth, D. W.: Geochemical constraints on initial and final depths of melting beneath mid-ocean ridges, J. Geophys. Res. Solid Earth, 100, 2211–2237, 1995.

Sim, S. J., Spiegelman, M., Stegman, D. R., and Wilson, C.: The influence of spreading rate and permeability on melt focusing beneath mid-ocean ridges, Phys. Earth Planet. Inter., 304, 106486, https://doi.org/10.1016/j.pepi.2020.106486, 2020.

Stolper, E.: The speciation of water in silicate melts, Geochim. Cosmochim. Ac., 46, 2609–2620, 1982.

Turner, S. J. and Langmuir, C. H.: Sediment and ocean crust both melt at subduction zones, Earth Planet. Sci. Lett., 584, 117424, https://doi.org/10.1016/j.epsl.2022.117424, 2022.

Tyburczy, J. A. and Roberts, J. J.: Low frequency electrical response of polycrystalline olivine compacts: Grain boundary transport, Geophys. Res. Lett., 17, 1985–1988, 1990.

Wallace, P. J.: Volatiles in subduction zone magmas: concentrations and fluxes based on melt inclusion and volcanic gas data, J. Volcanol. Geoth. Res., 140, 217–240, 2005.

White, R. S., Minshull, T.A., Bickle, M. J., and Robinson, C. J.: Melt generation at very slow-spreading oceanic ridges: Constraints from geochemical and geophysical data, J. Petrol., 42, 1171–1196, 2001.

641   Wu, K., Ling, M. X., Hu, Y. B., Guo, J., Jiang, X. Y., Sun, S. J., Liang, H. Y., Liu, X.,

642   and Sun, W. D.: Melt-fluxed melting of the heterogeneously mixed lower arc

643   crust: A case study from the Qinling orogenic belt, Central China, Geochem.

644   Geophys. Geosyst., 19, 1767–1788, 2018.
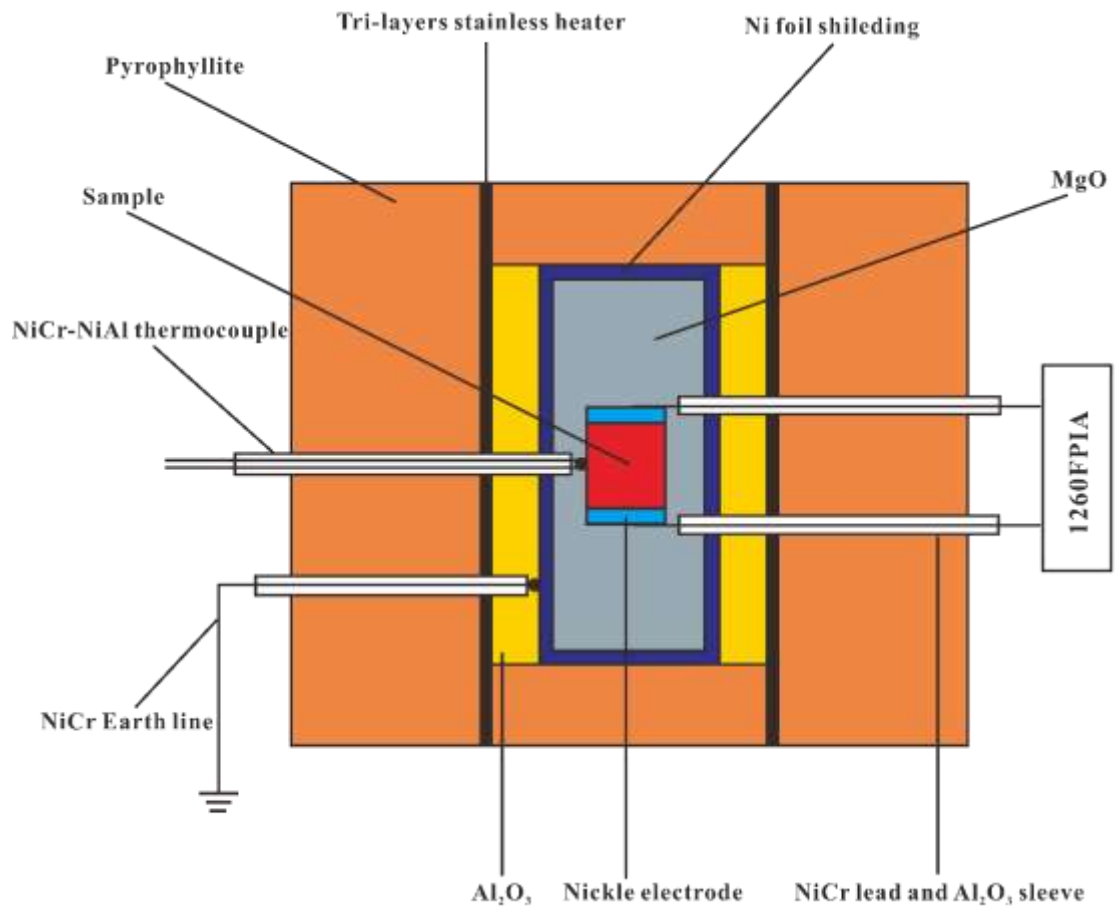
645

646 **Figure 1.** The experimental setup for the electrical conductivity measurements of

647 gabbroic melt at high temperatures and high pressures.

648
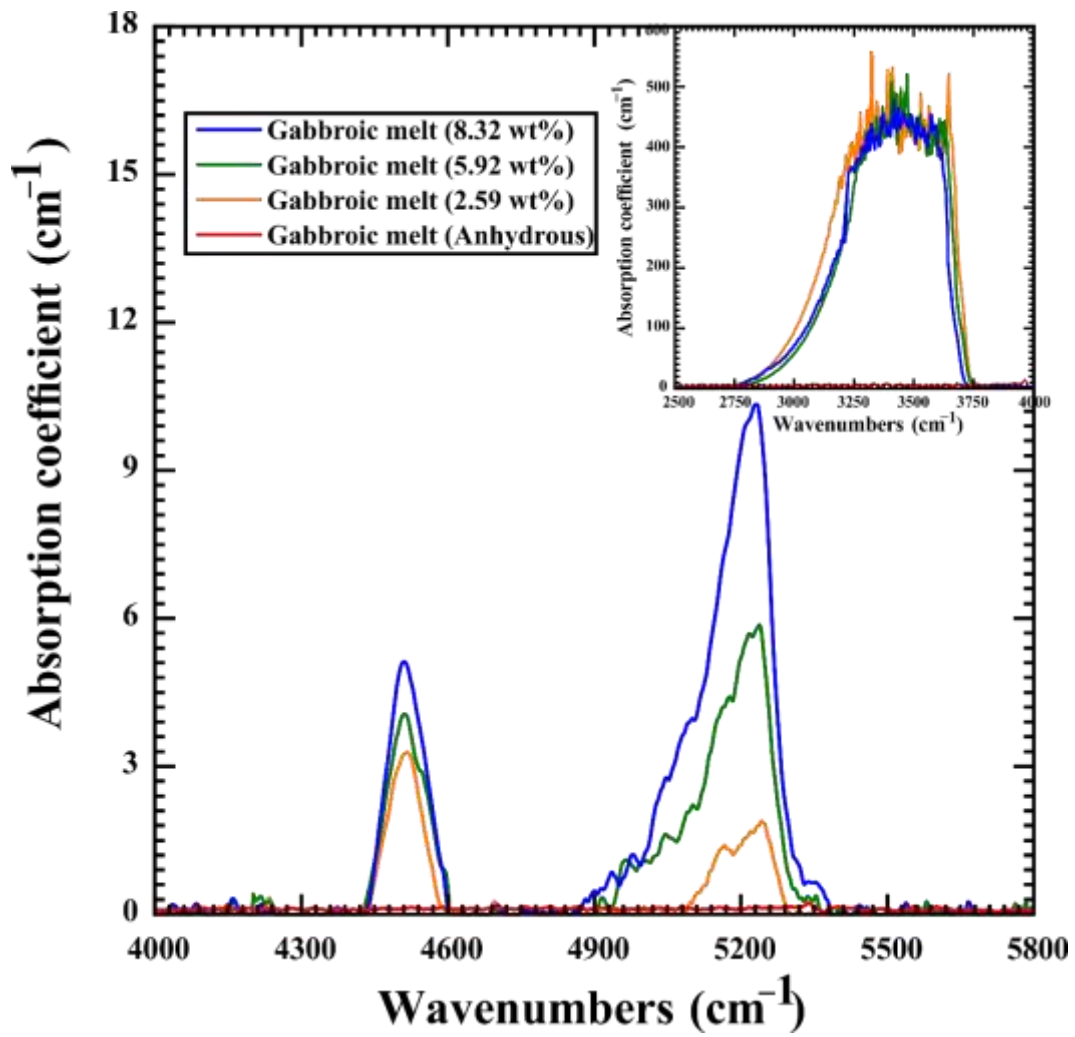
Figure 2. The representative FT–IR spectra of the gabbroic melt with various water

contents in the wavenumbers range of 4000–5800 cm^{-1} and 2500–4000 cm^{-1}.

651
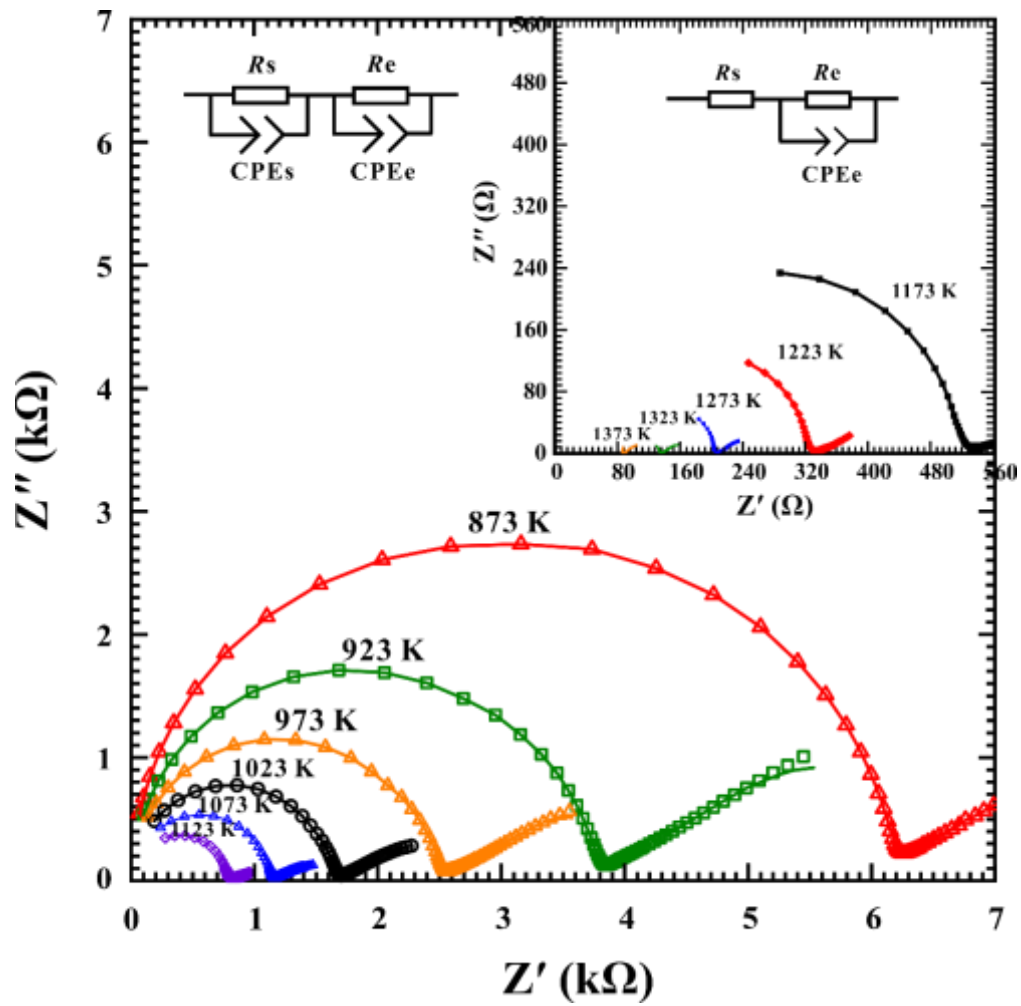
Figure 3. Typical complex impedance spectra for gabbroic melt (DW209) with a fixed water content of 2.59 wt% at temperatures of 873–1373 K and pressure of 2.0 GPa in the frequency range from 10^0 Hz to 10^6 Hz. The fitting results for the experimental data are displayed by using the solid line.
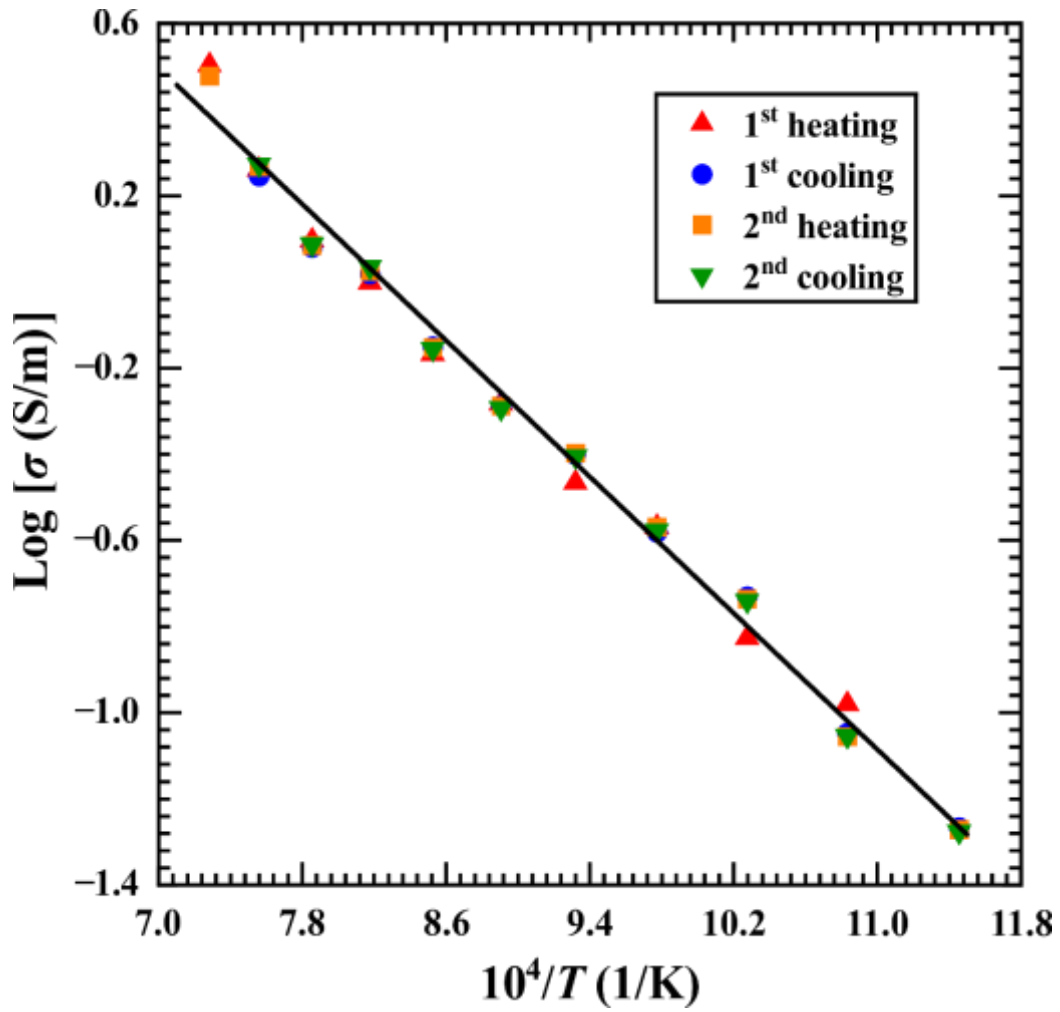
656

657 **Figure 4.** The electrical conductivity of gabbroic melt (DW212) with a fixed water

658 content of 2.59 wt% among two heating–cooling cycles at a pressure of 3.0 GPa.

659
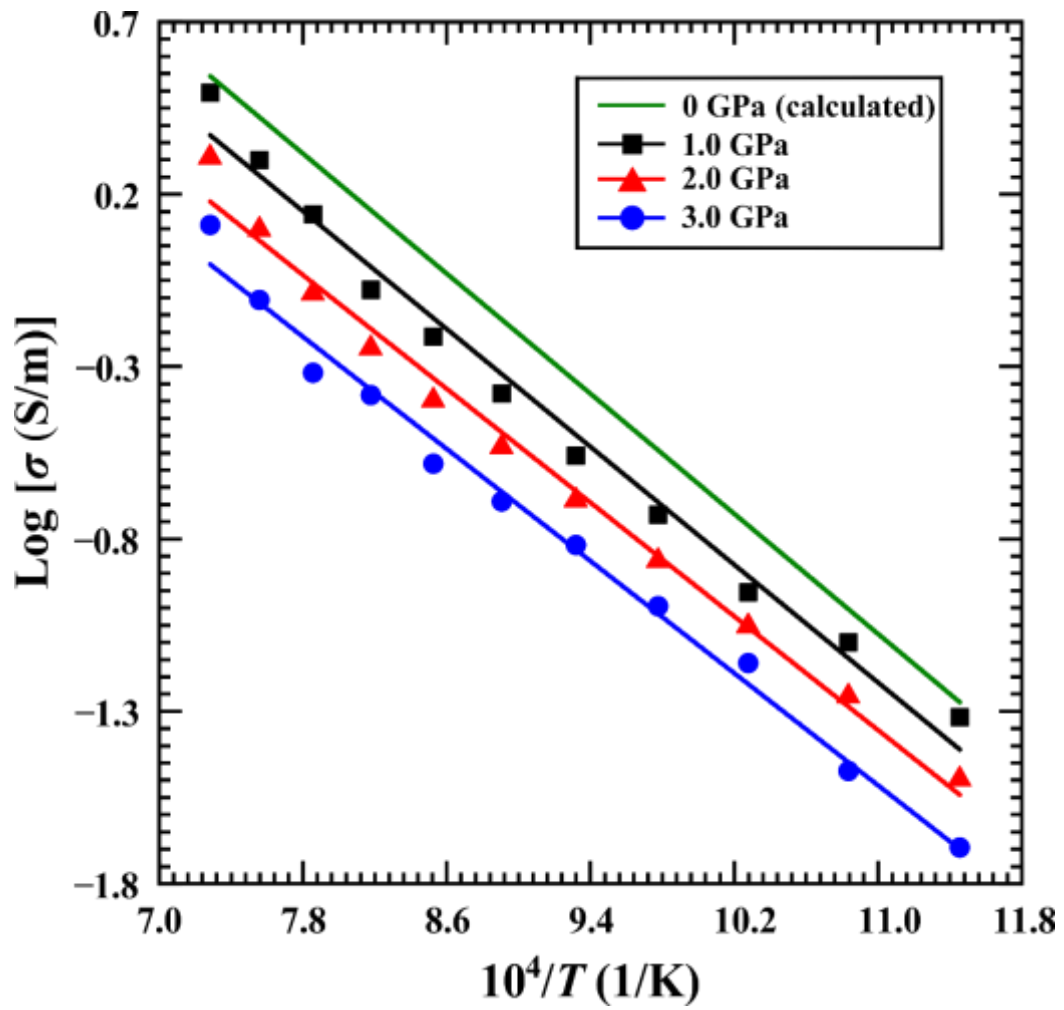
Figure 5. Influence of pressure on the electrical conductivity of gabbroic melt with a
fixed water content of 2.59 wt% at the temperature ranges of 873–1373 K.

662
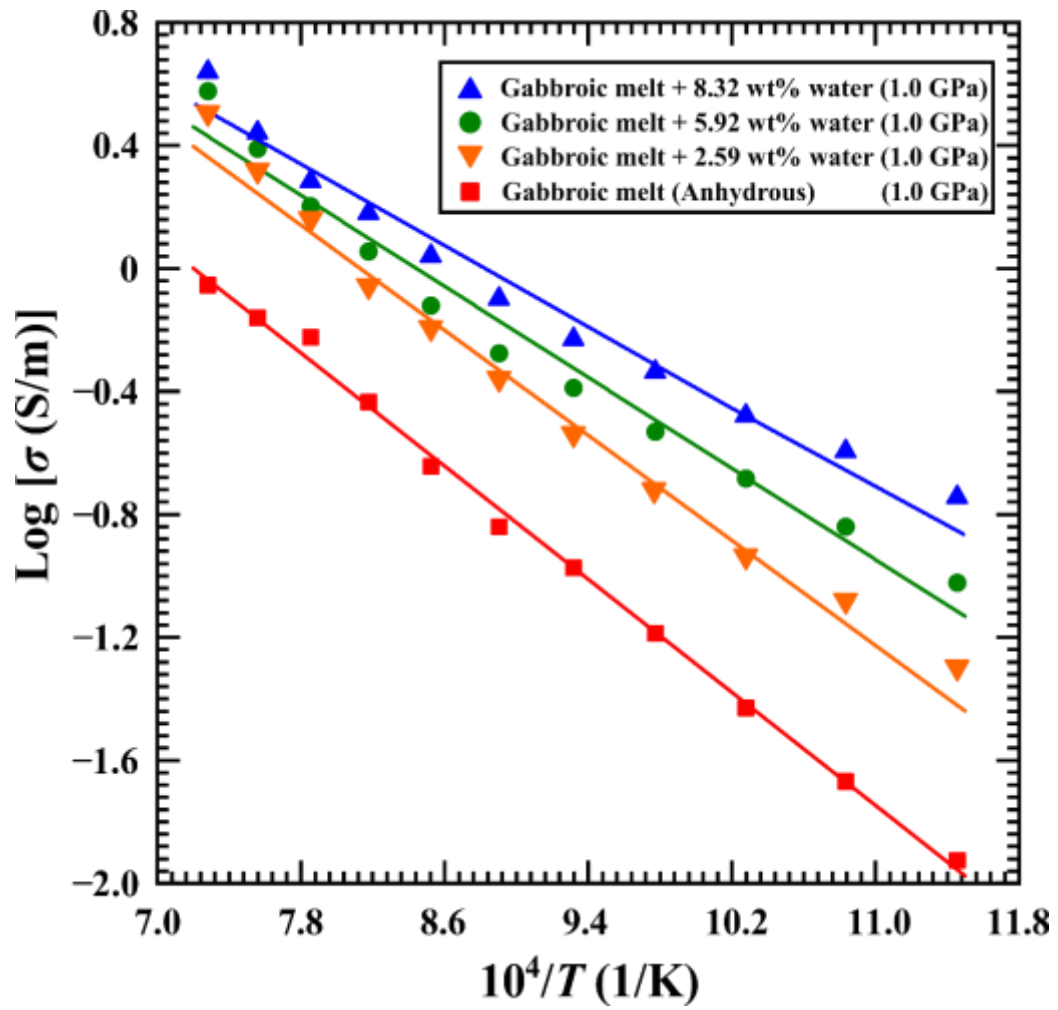
Figure 6. Logarithmic electrical conductivity of gabbroic melts with four different water contents as a function of reciprocal temperature at conditions of 873–1373 K and 1.0 GPa.

666
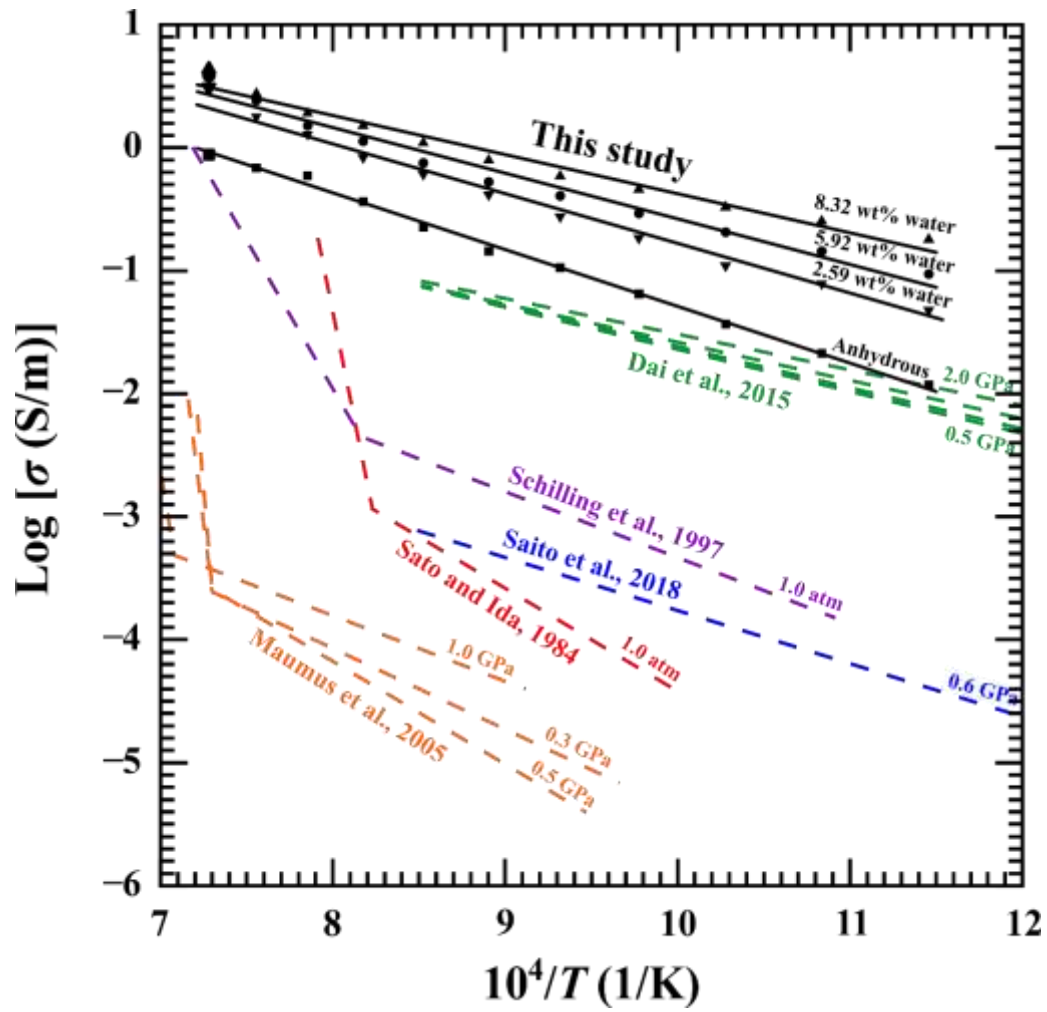
Figure 7. Comparison of electrical conductivity of gabbroic melts with the previously reported results from five natural gabbro samples at high–temperature and high–pressure conditions.

670
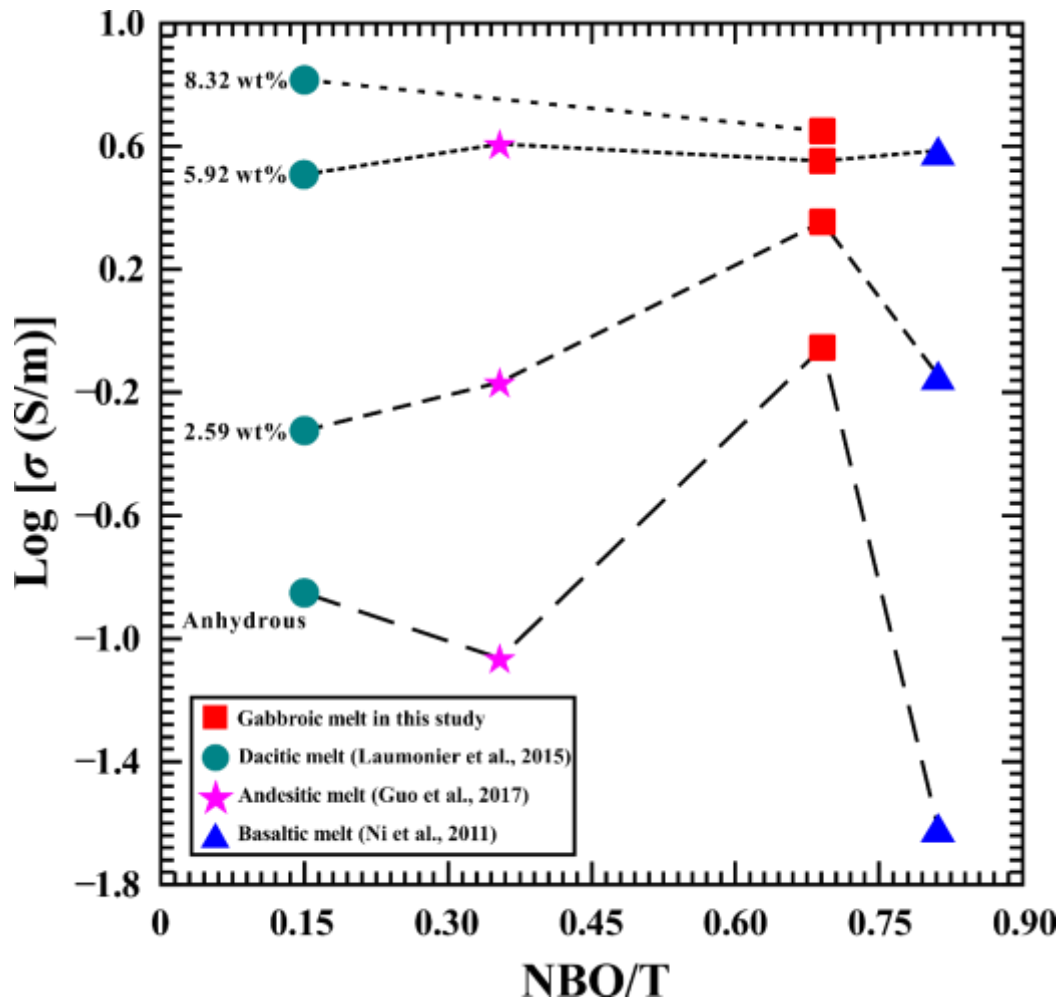
Figure 8. Variation of electrical conductivity of gabbroic melt and three representative calc–alkaline igneous rock melts with the degree of depolymerization (NBO/T) under conditions of four different water contents (i.e. 0, 2.59 wt%, 5.92 wt% and 8.32 wt%), 1373 K and 1.0 GPa. Data source: basaltic melt from Ni et al. (2011), andesitic melt from Guo et al. (2017), and dacitic melt from Laumonier et al. (2015).
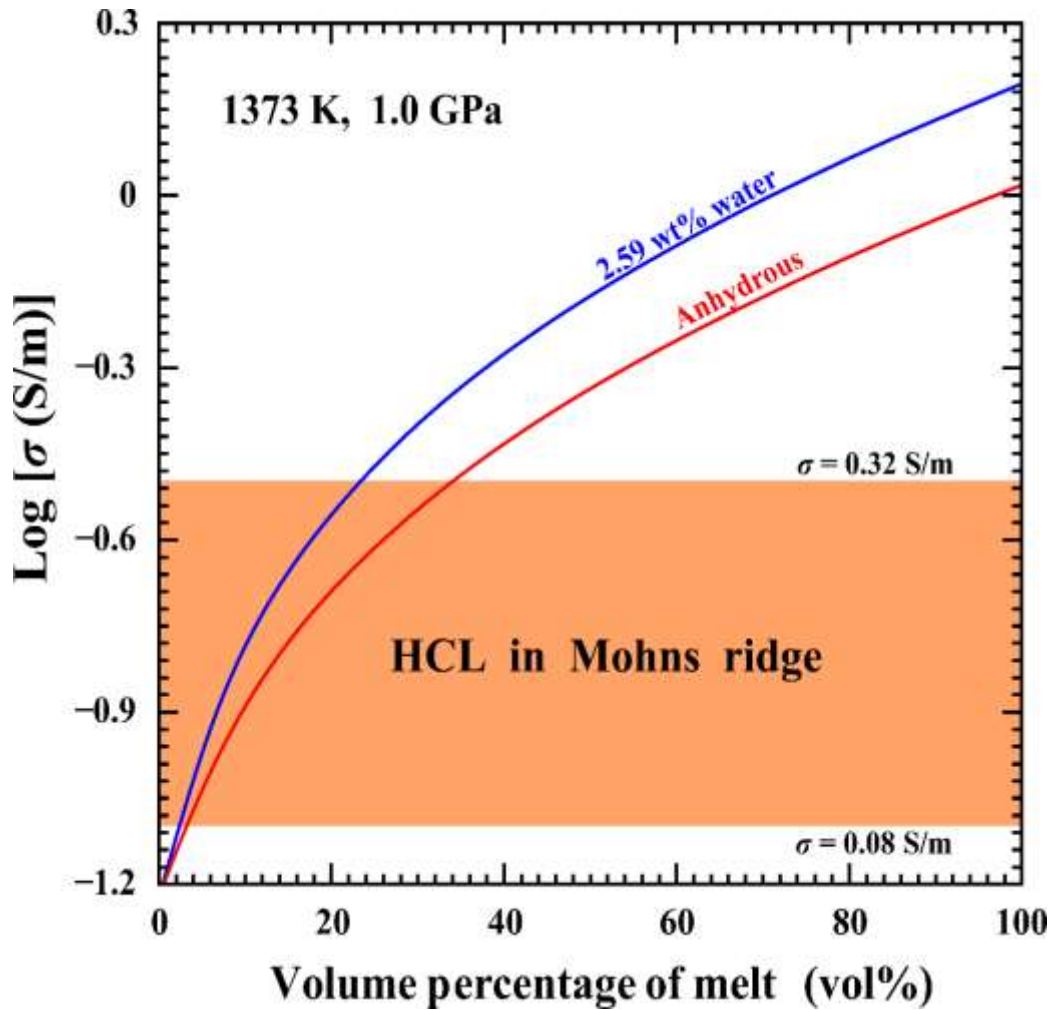
676

677 **Figure 9.** The electrical conductivity for the gabbroic melt–olivine system at
678 temperature of 1373 K and 1.0 GPa, calculated with Eq. 7 of the Hashin–
679 Shtrikman upper bound model. The electrical conductivity of olivine from Dai
680 and Karato (2014b) was adopted as $\sigma_{olivine}$. The orange region indicates the
681 gabbro layer within the electrical conductivity range of 0.08–0.32 S m^{-1} along
682 the ultraslow–spreading Arctic mid–ocean Mohns ridge region (Johansen et al.,
683 2019).

684 **Table 1.** The chemical composition of the gabbroic melts by virtue of the electronic

685 probe microscopy analysis (EPMA).

Sample	SiO_2	TiO_2	Al_2O_3	FeO	MnO	MgO	CaO	Na_2O	K_2O	Total (wt%)	NBO/T
Gabbroic melt (anhydrous)	51.32	0.56	12.37	9.93	0.20	11.06	11.82	2.15	0.50	99.91	0.6911
Gabbroic melt (2.59 wt% water)	51.22	0.55	12.40	9.92	0.18	11.29	11.72	2.19	0.48	99.95	0.6854
Gabbroic melt (5.92 wt% water)	51.23	0.57	12.40	9.87	0.18	11.28	11.70	2.21	0.47	99.91	0.6869
Gabbroic melt (8.32 wt% water)	51.22	0.57	12.40	9.88	0.17	11.27	11.69	2.21	0.46	99.86	0.6938

686

687 **Table 2.** Fitted parameters of Arrhenius relation for the electrical conductivity of

688 hydrous and anhydrous gabbroic melts under conditions of 873–1373 K and 1.0–3.0

689 GPa.

Sample	T (K)	P (GPa)	Water content Before experiment (wt%)	Water content After experiment (wt%)	Log σ_0 (σ_0 in S m^{-1})	ΔH (eV)
DW201	873–1373	1.0	8.32 ± 0.02	8.30 ± 0.01	2.80 ± 0.16	0.63 ± 0.03
DW204	873–1373	1.0	5.92 ± 0.01	5.90 ± 0.02	3.13 ± 0.18	0.74 ± 0.04
DW208	873–1373	1.0	2.59 ± 0.01	2.57 ± 0.01	3.48 ± 0.15	0.85 ± 0.03
DW209	873–1373	2.0	2.59 ± 0.03	2.58 ± 0.01	3.18 ± 0.13	0.83 ± 0.03
DW212	873–1373	3.0	2.59 ± 0.01	2.50 ± 0.02	2.79 ± 0.11	0.81 ± 0.03
DW210	873–1373	1.0	0	0	3.31 ± 0.08	0.93 ± 0.02

690

691   **Table 3.** Parameter values for the electrical conductivity of gabbroic melt with water

692   content of 2.59 wt% at pressures of 1.0–3.0 GPa. The equation $\sigma = \sigma_0 \cdot \exp(-\frac{\Delta U + P\Delta V}{kT})$

693   is adopted for the globally fitting of electrical conductivity data. In consideration of

694   a strong dependence of the pre–exponential factor (σ_0) on the pressure, we used the

695   relation $\sigma_0 = A_0 \cdot (1 - BP)$.

σ_0 (S m^{-1})	B (GPa^{-1})	ΔU (eV)	ΔV (cm^3 mole^{-1})
$A_0 = 2623.27 \pm 1.41$	$B = 0.22 \pm 0.03$	0.87 ± 0.04	-1.98 ± 0.52

696

697 **Table 4.** Parameter values for the electrical conductivity of gabbroic melts with

698 different water contents under conditions of 873–1373 K and 1.0 GPa. The

699 equation $\sigma = (A_1 + A_2 \cdot C_w^r) \cdot \exp(\frac{-\Delta H_0 - \alpha C_w^\beta}{RT})$ is adopted for the globally fitting of electrical

700 conductivity data.

A_1 (S m^{-1})	A_2 (S m^{-1})	ΔH_0 (eV)	α	β	r
6760±234	66069±240	1.03±0.04	34.85±2.24	17.70±1.31	0.43±0.05

701